

Spin polarization in a T-shape conductor induced by strong Rashba spin-orbit coupling

Masayuki Yamamoto¹, Tomi Ohtsuki² and Bernhard Kramer¹

¹ *I.Institut für Theoretische Physik, Universität Hamburg,
Jungiusstraße 9, 20355 Hamburg, Germany*

² *Department of Physics, Sophia University,
Kioi-cho 7-1, Chiyoda-ku, Tokyo 102-8554, Japan*

(Dated: February 13, 2019)

Abstract

We investigate numerically the spin polarization of the current in the presence of Rashba spin-orbit interaction in a T-shaped conductor as proposed by A.A. Kiselev and K.W. Kim (Appl. Phys. Lett. **78** 775 (2001)). The recursive Green function method is used to calculate the three terminal spin dependent transmission probabilities. We focus on single-channel transport and show that the spin polarization becomes nearly 100 % with a conductance close to e^2/h for sufficiently strong spin-orbit coupling. From the quantum dynamics of wave packets, we deduce that this is due to spin separation caused by quantum mechanical scattering at the junction. The influence of the disorder on the predicted effect is discussed.

PACS numbers:

I. INTRODUCTION

Recently, spin-dependent electronic transport is attracting considerable attention because of possible applications in spintronics [1, 2]. Many of the proposals for two dimensional (2D) spintronic devices are based on the presence of spin-orbit coupling in the 2D electron system (2DES) semiconductor heterostructure. There are two types of spin-orbit coupling terms in such systems. One is the so-called Dresselhaus term which originates from the inversion asymmetry of the zinc-blende structure [3]. The other is described by the Rashba Hamiltonian,

$$\mathcal{H}_R = \frac{\alpha}{\hbar}(\sigma_x p_y - \sigma_y p_x) \quad (1)$$

where α denotes the strength of spin-orbit coupling, σ_i and p_i ($i = x, y$) are the Pauli matrices and the components of the momentum, respectively. The Rashba mechanism is due to the effective electric field originating in the asymmetry of the potential confining the 2DES [4, 5].

It is well known that the Rashba term dominates in narrow-gap semiconductors while the Dresselhaus term is dominant in wide-gap systems [6]. Since the strength of the Rashba term can be controlled via external gates [7, 8], 2DES with Rashba spin-orbit interaction have become most promising for spintronic applications.

In order to realize such devices, one needs spin polarized electrons in the semiconductor inversion layer. Most straightforwardly, one could generate spin polarized electrons by attaching ferromagnetic metallic contacts to the 2DES and injecting a current [9]. However, it has been found that in practice the efficiency of the spin injection from a ferromagnet into a semiconductor is very poor because of the conductivity mismatch [10]. Thus, alternative methods have to be invented. Since strong spin-orbit scattering can lead to spatially inhomogeneous spin polarization [11] the generation of spin polarized electrons via spin-orbit coupling is in principle possible.

In this paper we consider a conductor with a T-shape structure with Rashba spin-orbit coupling as originally proposed by Kiselev and Kim [12]. For relatively small strength of the spin-orbit coupling, these authors have obtained high spin polarization. However, the corresponding conductance has been found to be very small. This problem of the small conductance has been eventually overcome by considering a ring-shape electron resonator [13]. It has also been reported that spin accumulation can occur for considerably strong

spin-orbit coupling in a quasi-1D wire [14].

In both of the above cases, mainly electron transport in the lowest subband (single-channel transport) has been considered. Due to the self-duality of scattering matrix [15] for the system with spin-orbit interaction, no spin polarization of the current can be obtained for single-channel transport in two-terminal devices. Therefore, one has to consider at least a conductor with three terminal. The single-channel limit seems to be ideal because one can completely suppress the effect of the D'yakonov-Perel' relaxation, which is the major spin relaxation mechanism in such systems [16]. We will show that the amplitude of the spin polarization becomes almost perfect with only very little loss of the conductance if the spin-orbit interaction is sufficiently strong. We argue that the predicted effect should be experimentally accessible in InAs.

In the next section, we describe the model system to be investigated numerically. We use the Ando tight-binding Hamiltonian with Rashba coupling in the off-diagonal matrix elements [17]. In Sec. III, the results for the dependence of the polarization on the energy and the strength of spin-orbit coupling are presented. The amplitude of spin polarization is shown to depend on the ratio between the π -phase spin precession length and the width of the quantum wires of the T-shape conductor. In Sec. IV, we discuss the origin of the polarization by using the results of numerical simulations of the dynamics of an injected wave packet. The effect of disorder is also investigated. The final section is devoted to summary and discussion.

II. THE MODEL

We consider the T-shape conductor shown in Fig.1 in the presence of Rashba spin-orbit coupling. The sample region is connected to three electron reservoirs by ideal leads. Electron current is injected into the sample from the reservoir 1 and goes to reservoirs 2 or 3. At small voltages, the currents I_{12} and I_{13} from reservoir 1 to reservoirs 2 and 3, respectively, are proportional to the conductances G^{12} and G^{13} .

The Rashba spin-orbit coupling can be described in the tight-binding language by the Ando Hamiltonian [17],

$$\mathcal{H} = \sum_{i,\sigma} W_i c_{i\sigma}^\dagger c_{i\sigma} - \sum_{\langle i,j \rangle, \sigma, \sigma'} V_{i\sigma, j\sigma'} c_{i\sigma}^\dagger c_{j\sigma'}, \quad (2)$$

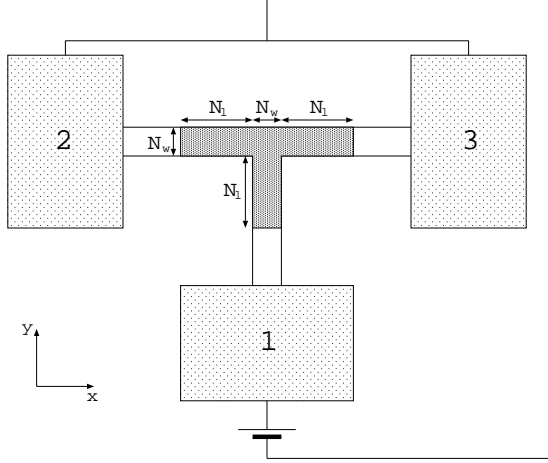


FIG. 1: Scheme of the T-shaped conductor. Current injected from reservoir 1 can go to reservoirs 2 or 3. Shaded: regions with non-vanishing spin-orbit coupling; parameters: $N_w = 10a$ and $N_l = 20a$ (a a lattice spacing of tight binding model).

where

$$V_{i,i+\hat{x}} = V_0 \begin{pmatrix} \cos \theta & -\sin \theta \\ \sin \theta & \cos \theta \end{pmatrix}, \quad (3)$$

and

$$V_{i,i+\hat{y}} = V_0 \begin{pmatrix} \cos \theta & i \sin \theta \\ i \sin \theta & \cos \theta \end{pmatrix}. \quad (4)$$

Here, $c_{i\sigma}^\dagger (c_{i\sigma})$ denotes the creation (annihilation) operator of an electron on site i with spin σ , W_i the random potential on the site i distributed uniformly in $[-W/2, W/2]$, and $V_{i,i+\hat{x}} (V_{i,i+\hat{y}})$ the hopping matrix elements in x -(y -) directions. The hopping is restricted to nearest neighbours. The hopping energy $V_0 = \hbar^2/2m^*a^2$, where m^* is the effective electron mass and a the tight binding lattice spacing, is taken as the unit of the energy. The parameter θ represents the strength of the spin-orbit coupling and is related to Rashba coupling α by

$$\alpha \simeq 2\theta V_0 a \quad (\text{for } \theta \ll 1). \quad (5)$$

The conductance between reservoirs j to i [18] and the corresponding spin polarization are defined by

$$G^{ij} = G_0 \text{Tr} t_{ij}^\dagger t_{ij}, \quad (6)$$

and

$$P_k^{ij} = \frac{\text{Tr} t_{ij}^\dagger \sigma_k t_{ij}}{\text{Tr} t_{ij}^\dagger t_{ij}} \quad (k = x, y, z), \quad (7)$$

with the conductance quantum $G_0 \equiv e^2/h$, t_{ij} denoting the transmission matrix between reservoirs j and i . Below, we will focus on the transport between reservoirs 1 and 2. Transport between reservoirs 1 and 3 can trivially be deduced via current conservation and the symmetry of the system.

We calculate the amplitude of the total spin polarization defined by

$$|\mathbf{P}| = (P_x^2 + P_y^2 + P_z^2)^{1/2}, \quad (8)$$

instead of only the z -component, since no spin quantization axis exists when only spin-orbit coupling is present.

As described in detail in Appendix A, we can obtain the transmission coefficient $t_{\mu\nu}^{IJ}$ for the incident channel ν with velocity v_ν in the probe J and out-going channel μ with velocity v_μ in the probe I as [19]

$$t_{\mu\nu}^{IJ} = \left(\frac{v_\mu}{v_\nu}\right)^{1/2} [-(U^I)^{-1}G^{IJ}U^J\{(\Lambda^J)^{-1} - \Lambda^J\}]_{\mu\nu} \quad (9)$$

where G^{IJ} is the part of Green function corresponding to the transport from the probe J to I . Λ^J contains only diagonal elements, $\Lambda^J(i, j) = \lambda_i^J \cdot \delta_{ij}$, where λ_i^J is the i -th eigenvalue of the transfer matrix for an ideal region in the probe J and $U^{I(J)}$ consists of the set of eigenfunctions for $\{\lambda_i^{I(J)}\}$.

III. RESULTS

By using the recursive Green function method, we calculate the amplitude of the spin polarization. For the system size we assume $N_w = 10a$ and $N_l = 20a$. We first consider an clean system ($W = 0$).

Figure 2 shows the dependence of the conductance and the spin polarization on the Fermi energy E for weaker and stronger spin-orbit coupling. We consider the energy region for single-channel transport. For weaker spin-orbit coupling ($\theta = 0.02\pi$), high spin polarization is obtained for energies just before the second channel is opened ($E \simeq -3.68V_0$). The corresponding conductance is small as compared to G_0 [12]. Almost perfect polarization is obtained together with a conductance close to G_0 for stronger spin-orbit coupling ($\theta = 0.06\pi$). Here, the polarization is almost insensitive to the energy except near the band edge.

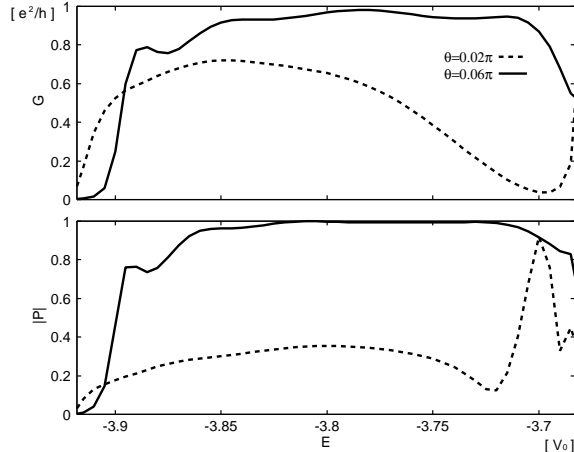


FIG. 2: Conductance G and spin polarization $|P|$ as functions of the Fermi energy E in the region of single-channel transport. Almost 100% polarization is obtained together with $G \approx G_0$ for stronger spin-orbit coupling ($\theta = 0.06\pi$). For $\theta = 0.02\pi$ high polarization is obtained only at energies just before the second channel opens.

Figure 3 shows the dependence of the conductance and the spin polarization on the strength of spin-orbit coupling at energy $E = -3.8V_0$. With increasing strength of the spin-orbit coupling, P_y also increases monotonically while P_x and P_z oscillate. We also note that the conductance increases together with the amplitude of the polarization. Due to the symmetry of the T-shaped conductor, the current into reservoir 3 has the same polarization in the direction of y but opposite polarizations in x - and z -directions [12].

What are the conditions for achieving almost perfect polarization? We define the π -phase spin precession length $L_{so}(|P|, N_w) = \pi a / 2\theta(|P|, N_w)$ where $\theta(|P|, N_w)$ is the spin-orbit coupling strength. From the plot $L_{so}(|P|, N_w)$ as a function of the width of the system N_w (Fig. 4) one concludes that $L_{so}(|P|, N_w)$ is almost linear in N_w and high polarization, $|P| > 0.99$, is achieved for $L_{so}(|P|, N_w) < N_w$. On the other hand, no dependence on the length of the leads (N_l) is observed as shown in Fig.5.

IV. WAVE PACKET DYNAMICS

In order to physically understand the origin of the polarization, we have performed numerical simulations of the time evolution of a wave packet in our model by using the equation-of-motion method [20, 21].

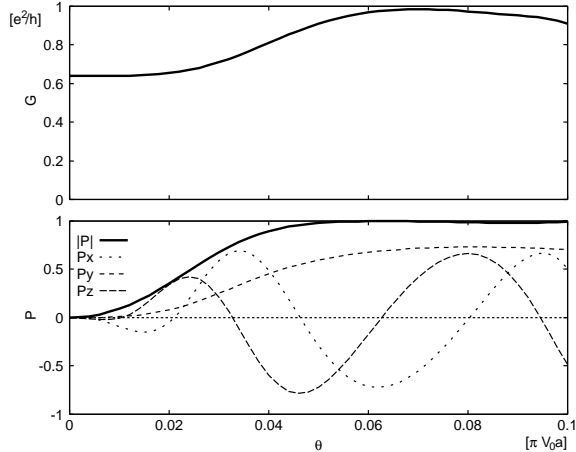


FIG. 3: Conductance G and spin polarization P_k in the directions of $k = x, y, z$ as functions of the strength of spin-orbit coupling θ for $E = -3.8V_0$; P_y increases monotonically with increasing θ while P_x and P_z oscillate.

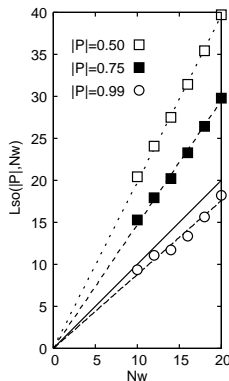


FIG. 4: The spin precession lengths L_{so} for $|P| = 0.5, 0.75, 0.99$ as functions of the width of the wires N_w for $E = -3.8V_0$. The polarization becomes almost perfect if the spin precession length becomes shorter than the wire width, $L_{\text{so}}(|P|, N_w) = \pi a / 2\theta(|P|, N_w) < N_w$. Solid line: $L_{\text{so}}(|P|, N_w) = N_w$ corresponding to $|P| \simeq 0.97$.

A. The equation-of-motion method

The method is based on a higher-order decomposition of the exponential operators proposed originally by Suzuki [22].

Starting point is the preparation of the initial state of a wave packet as shown in Fig. 6. The time evolution of this wave packet is displayed in Figs. 7 to 10. The charge density and

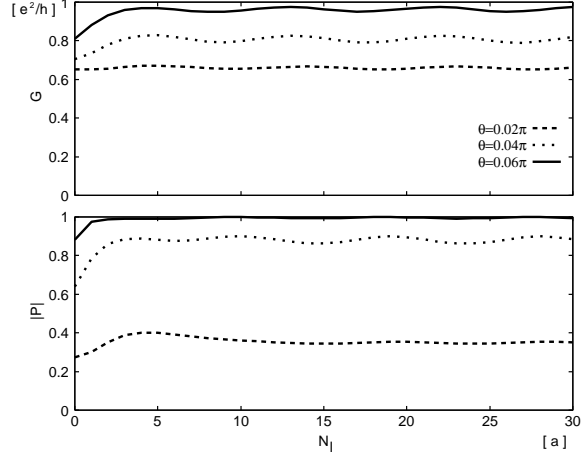


FIG. 5: Conductance G and spin polarization $|P|$ as functions of the wire length N_l for several strengths of the spin-orbit coupling at $E = -3.8V_0$. The polarizations are insensitive to the length of leads.

the spin polarization are given by

$$\rho = \sum_{\sigma=\uparrow,\downarrow} (|\langle \uparrow | \psi_\sigma \rangle|^2 + |\langle \downarrow | \psi_\sigma \rangle|^2), \quad (10)$$

and

$$P_k = \sum_{\sigma=\uparrow,\downarrow} (|\langle \uparrow_k | \psi_\sigma \rangle|^2 - |\langle \downarrow_k | \psi_\sigma \rangle|^2) \quad (11)$$

respectively, with $k = x, y, z$ denoting the components, and \uparrow_k (\downarrow_k) representing the spin parallel (antiparallel) to the k -direction. In the following, the index k is omitted if we consider the z -component. We calculate the spin polarizations along the x - and y -directions.

The initial wave packet with spin σ is assumed as

$$\psi_\sigma(t=0) = A \sin(k_x x) \exp\left(ik_y y - \frac{\Delta k_y^2 y^2}{4}\right) \chi_\sigma, \quad (12)$$

with

$$\chi_\uparrow = \begin{pmatrix} 1 \\ 0 \end{pmatrix}, \quad \chi_\downarrow = \begin{pmatrix} 0 \\ 1 \end{pmatrix}. \quad (13)$$

We assume $k_x = \pi/(N_w + a)$ corresponding to the lowest subband and $k_y = 0.35a^{-1}$ with $\Delta k_y = 0.15a^{-1}$. For the strength of spin-orbit coupling we have assumed $\theta = 0.06\pi$ and for the system size $N_w = 10a$ and $N_l = 20a$. The single time step Δt is assumed to be $0.05\hbar V_0^{-1}$. Because of the different initial conditions, the results obtained from the Green

function method cannot be the same as those obtained from the equation-of-motion method. Nevertheless, we can interpret the former by considering the time evolution of the wave packet.

First we consider the polarization along the x -direction. The wave packet is negatively polarized before it is injected into the junction (Fig.7). This corresponds to the spin accumulation which occurs in a quasi-1D wire with a strong spin-orbit coupling [14]. This polarized spin precesses after entering the lead regions parallel to x -direction and gives rise to a rotating polarization in the x - z plane (Fig.9 and 10).

For polarization along the y -direction, we observe that spin separation occurs near the junction (Fig.8). This is because the group velocity depends on the spin σ_y . After the spins are separated, they begin to move to reservoirs 2 and 3. When the wave packets are still in the probes where the spin-orbit interaction is present, the polarization P_y can take both positive and negative values (Fig.9). However, the interface between the sample and the ideal lead acts as the spin-dependent potential wall and only $P_y > 0$ (< 0) is selected at the left (right) interface (Fig.10).

B. The influence of disorder

We now consider briefly the effect of disorder on the spin polarization (Fig.11). An ensemble average is performed over 10^4 samples. The suppression of the polarization by disorder becomes more prominent as the spin-orbit coupling becomes stronger. The mean free path of a 2DES in the tight-binding model is described by [19]

$$L_m = 48aV_0^{3/2} \frac{\sqrt{E + 4V_0}}{W^2}. \quad (14)$$

One can use this estimate to distinguish the ballistic regime from the diffusive one, we obtain $W \simeq 1.53V_0$ for $L_m = 50a$. As seen in the figure, the sample size must be smaller than the mean free path in order to obtain high spin polarization.

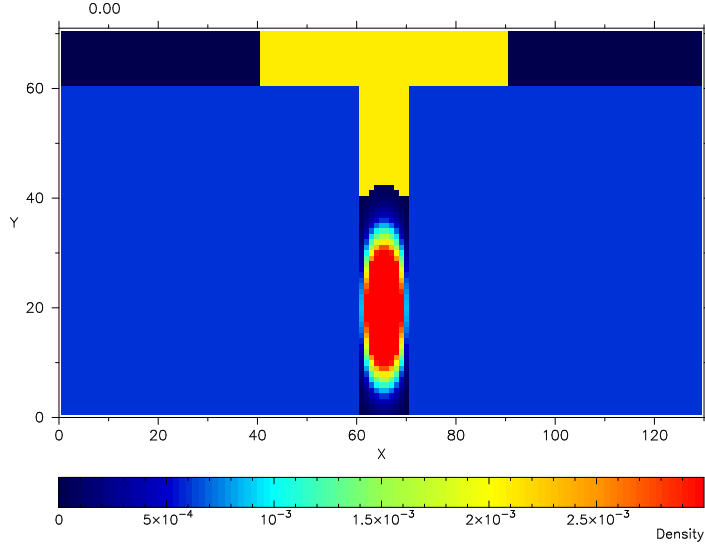


FIG. 6: Initial state of the wave packet ($t = 0$). Yellow: sample with spin-orbit coupling. The wave packet is injected along the y -direction.

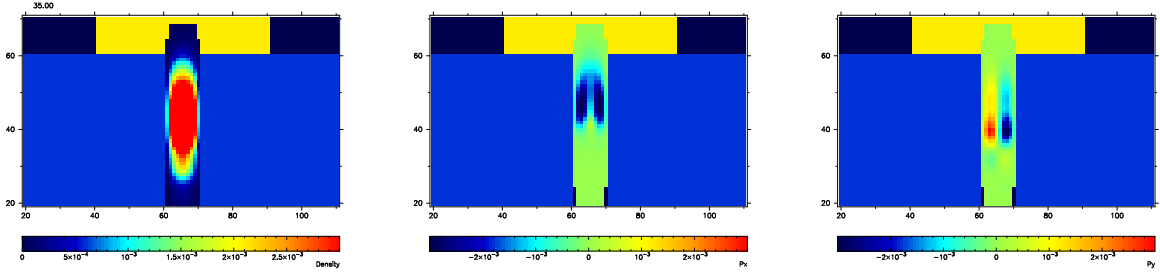


FIG. 7: The wave packet enters the sample region ($t = 35\hbar V_0^{-1}$). Left: charge density; center: spin polarization P_x ; right: spin polarization P_y . Spin accumulation occurs along the x -direction (center).

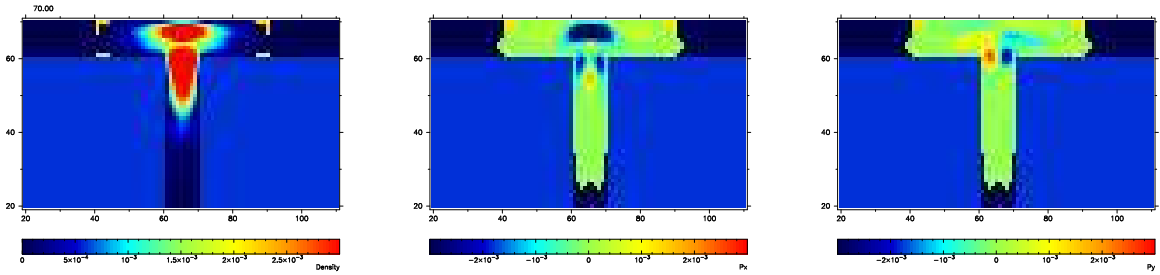


FIG. 8: The wave packet reaches the junction ($t = 70\hbar V_0^{-1}$). Left: charge density; center: spin polarization P_x ; right: spin polarization P_y . Spin separation occurs along the y -direction (right).

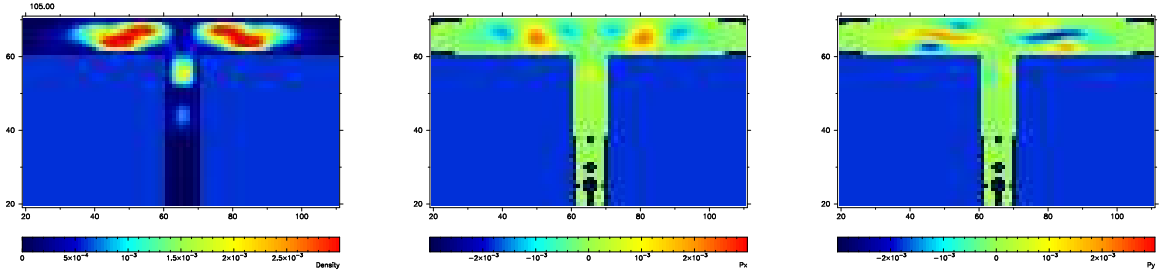


FIG. 9: The wave packet goes through the horizontal wire region ($t = 105\hbar V_0^{-1}$). Left: charge density; center: spin polarization P_x ; right: spin polarization P_y . Spins parallel to the x -direction precess along the wire (center) while those parallel to the y -direction do not (right).

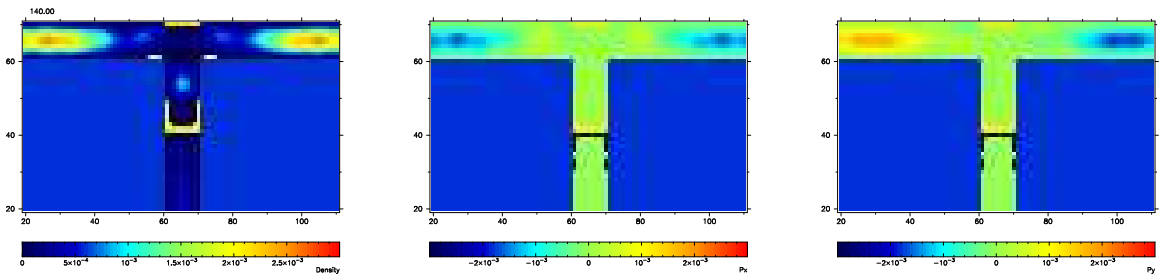


FIG. 10: The wave packet is going out from the sample region ($t = 140\hbar V_0^{-1}$). Left: charge density; center: spin polarization P_x ; right: spin polarization P_y . The interface between the sample and the ideal probe acts as spin-dependent potential wall for spins parallel to the y -direction (right).

C. The influence of other channels

Finally let us consider the system whose size is $N_w = 50a$ and $N_l = 50a$. Figure 12 shows the dependence of the conductance and the spin polarization on the Fermi energy E for $\theta = 0.01\pi$. The electron transport is multi-channel one in this energy region where the number of channels increases from 5 to 10. While the spin polarization is reduced by multi-channel transport it still stays higher than 10%. The mechanism of polarization should be more complicated than what we have given in this paper because our interpretation is suitable for single-channel transport.

V. SUMMARY AND DISCUSSION

In this paper we have investigated numerically spin polarized linear transport in a T-shaped conductor with Rashba spin-orbit coupling. We have considered single-channel trans-

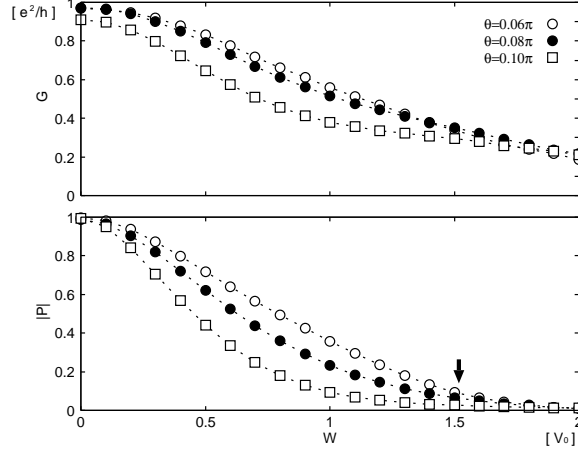


FIG. 11: Conductance G and spin polarization $|P|$ as functions of the strength of disorder W for several spin-orbit couplings at $E = -3.8V_0$. Ensemble average has been taken with 10^4 samples. For stronger spin-orbit coupling, the polarization is more sensitive to disorder. Arrow: crossover between ballistic and diffusive regimes [cf. Eq.(14)].

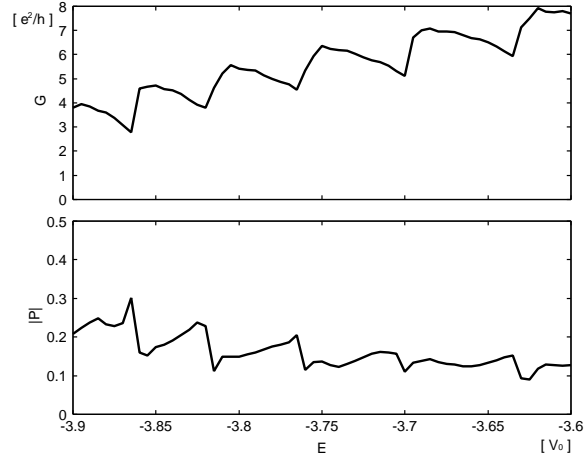


FIG. 12: Conductance G and spin polarization $|P|$ as functions of the Fermi energy E in the region of multi-channel transport. The system size is set to be $N_w = 50a$ and $N_l = 50a$, and the strength of spin-orbit coupling $\theta = 0.01\pi$. The number of channel increases from 5 to 10 in this energy region. The polarization keeps more than 10%.

port and found that the spin polarization becomes almost perfect with a conductance close to G_0 for stronger spin-orbit coupling. By numerically simulating the spin dependent dynamics of wave packets we have found that the spin accumulation in the wire region causes the spin polarization along the x - and z -directions. Near the junction, the group velocity of

the electrons becomes spin-dependent and spins with y -components become separated. We have found that the magnitude of the polarization depends on the ratio between the π -phase spin precession length and the wire width. If the precession length becomes shorter than the wire width, nearly 100% polarization can be achieved.

We have also investigated the effect of disorder on the polarization. Since the polarization becomes more sensitive to the disorder when the spin-orbit interaction is stronger, one needs to prepare the clean samples so that the system belongs to the ballistic regime, for obtaining perfect polarization of the current.

In order to obtain information whether or not the predicted effects are observable in experiment, let us consider the parameters required for one of the favorable materials, InAs, with an effective mass $m^* = 0.039m_0$ (m_0 is the free electron mass) and Rashba coupling $\alpha = 23.8 \times 10^{-12}$ eVm [23]. Let us assume that the width of the conduction band is $\Delta = 1$ eV. This gives for $V_0 = \Delta/2Z = 125$ meV ($Z = 4$ for square lattice), and for the lattice constant $a = \hbar/(2m^*V_0)^{1/2} \simeq 2.8$ nm. Using the above numerical value of α one obtains $\theta = \alpha/2V_0a \simeq 0.01\pi$. This would reduce the polarization to about 10%, still a reasonable value for being observable in experiment. The crucial point, however, is the condition that transport has to be in the one-channel regime. The wire width is about 20 nm for single-channel transport because Fermi energy is of the order of 10 meV. In principle it is possible to fabricate such a narrow wire, but it makes the mean free path shorter and the effect of disorder may become critical. On the other hand, the wire width becomes 140 nm for the system with $N_w = 50a$ (Sec.IV C). This width of quantum wire can be easily fabricated rather than that for single-channel transport while we need to investigate further the effect of disorder and D'yakonov-Perel' relaxation. The above discussion suggests that the spin polarization of the current in a T-shaped conductor without applying a magnetic field can be observed in experiment even for multi-channel transport.

Acknowledgments

We thank J. Nitta, J. Ohe, K. Dittmer and K. Slevin for fruitful discussions. This work was supported by SFB 508 "Quantenmaterialien" of the Deutsche Forschungsgemeinschaft, and by the Marie-Curie Network MCRTN-CT2003-504574 of the EU.

APPENDIX A: RECURSIVE GREEN FUNCTION METHOD FOR MULTI-TERMINAL GEOMETRY

For numerical calculations, we apply the recursive Green function method[19] to the case of multi-terminal geometry. Let us consider three terminal geometry described in Fig.13. The central sample region (C) is attached to three probes (D , R and L). Each probe consists of the infinite ideal region and the sample one whose size is $N_p \times N_w^I$ ($I = D, R$ and L).

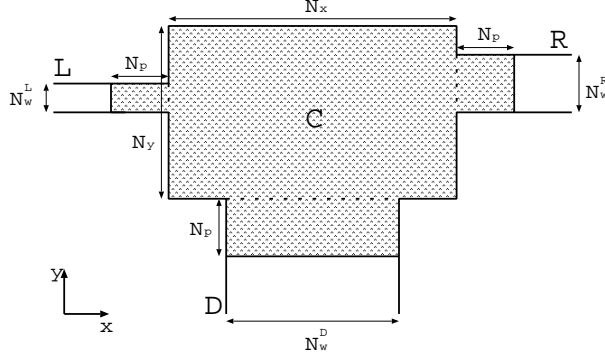


FIG. 13: Schematic draw of three terminal geometry. The shaded area represents a sample region where spin-orbit interaction is present. This sample region is connected to three electron reservoirs by ideal probes.

The full Hamiltonian can be written down as

$$\tilde{\mathcal{H}} = \begin{pmatrix} \tilde{\mathcal{H}}_{N_p+1} & -V_{N_p+1, N_p} & 0 & \cdots & 0 & 0 & 0 \\ -V_{N_p+1, N_p}^\dagger & \mathcal{H}_{N_p} & -V_{N_p, N_p-1} & \cdots & 0 & 0 & 0 \\ 0 & -V_{N_p, N_p-1}^\dagger & \mathcal{H}_{N_p-1} & \cdots & 0 & 0 & 0 \\ \vdots & \vdots & \vdots & \ddots & \vdots & \vdots & \vdots \\ 0 & 0 & 0 & \cdots & \mathcal{H}_2 & -V_{2,1} & 0 \\ 0 & 0 & 0 & \cdots & -V_{2,1}^\dagger & \mathcal{H}_1 & -V'_{1,C} \\ 0 & 0 & 0 & \cdots & 0 & -V'^\dagger_{1,C} & \mathcal{H}^C \end{pmatrix}. \quad (\text{A1})$$

\mathcal{H}^C is the Hamiltonian for the central sample region and can be described by

$$\mathcal{H}^C = \begin{pmatrix} \mathcal{H}_1^C & -V_{12}^C & 0 & \cdots & 0 \\ -V_{21}^C & \mathcal{H}_2^C & -V_{23}^C & \cdots & 0 \\ 0 & -V_{32}^C & \mathcal{H}_3^C & \cdots & 0 \\ \vdots & \vdots & \vdots & \ddots & \vdots \\ 0 & 0 & 0 & \cdots & \mathcal{H}_{N_x}^C \end{pmatrix}, \quad (\text{A2})$$

where \mathcal{H}_i^C denotes the Hamiltonian for the i -th slice along the y -direction and V_{ij}^C the hopping term between the slice i and j . The hopping is restricted to nearest neighbours. $V_{1,C}^C$ is the hopping term between the central sample region and its neighbouring slices of three probes. \mathcal{H}_i is the Hamiltonian for the set of i -th slices of three probes and can be described by

$$\mathcal{H}_i = \begin{pmatrix} \mathcal{H}_i^D & 0 & 0 \\ 0 & \mathcal{H}_i^R & 0 \\ 0 & 0 & \mathcal{H}_i^L \end{pmatrix}, \quad (\text{A3})$$

where \mathcal{H}_i^I ($I = D, R$ and L) is the Hamiltonian for the i -th slice of the probe I (see Fig.14). V_{ij} is the hopping term between the set of i -th slices and j -th ones.

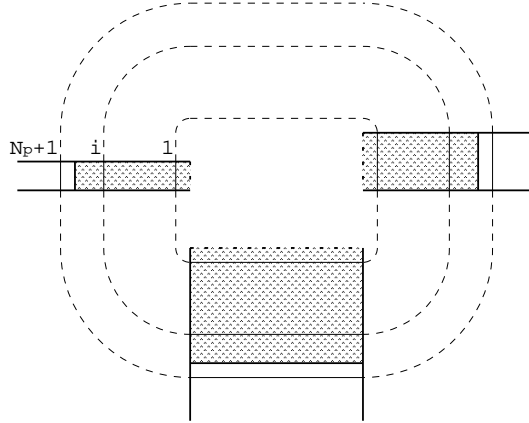


FIG. 14: Graphical interpretation for the Hamiltonian \mathcal{H}_i . The i -th slices of three probes are gathered.

Let us define some variables by following Ref.[19] as

$$\Lambda^I = \begin{pmatrix} \lambda_1^I & & \\ & \ddots & \\ & & \lambda_{N_w^I}^I \end{pmatrix}, \quad (\text{A4})$$

and

$$U^I = \left(\mathbf{u}_1^I \cdots \mathbf{u}_{N_w^I}^I \right), \quad (\text{A5})$$

where $\lambda_1^I, \dots, \lambda_{N_w^I}^I$ are the eigenvalues of transfer matrix for the ideal region on the probe I and $\mathbf{u}_1^I, \dots, \mathbf{u}_{N_w^I}^I$ the eigenfunctions corresponding to $\lambda_1^I, \dots, \lambda_{N_w^I}^I$. We note that the incoming solutions and outgoing ones have the same form when there is no magnetic field. Then the effective Hamiltonian on site $N_p + 1$ for the probe I can be written by

$$\tilde{\mathcal{H}}_{N_p+1}^I = \mathcal{H}_{N_p+1}^I - V_0 F^I, \quad (\text{A6})$$

with

$$F^I = U^I \Lambda^I (U^I)^{-1}, \quad (\text{A7})$$

where V_0 is the hopping term in the ideal probe. $\tilde{\mathcal{H}}_{N_p+1}^I$ can be obtained by exchanging \mathcal{H}_i^I for $\tilde{\mathcal{H}}_i^I$ in Eq.(A3) and setting $i = N_p + 1$.

We define corresponding Green function as

$$G \equiv \frac{1}{E - \tilde{\mathcal{H}}} = \begin{pmatrix} G_{N_p+1, N_p+1} & G_{N_p+1, N_p} & \cdots & G_{N_p+1, 1} & G_{N_p+1, C} \\ G_{N_p, N_p+1} & G_{N_p, N_p} & \cdots & G_{N_p, 1} & G_{N_p, C} \\ \vdots & \vdots & \ddots & \vdots & \vdots \\ G_{1, N_p+1} & G_{1, N_p} & \cdots & G_{1, 1} & G_{1, C} \\ G_{C, N_p+1} & G_{C, N_p} & \cdots & G_{C, 1} & G_{C, C} \end{pmatrix}. \quad (\text{A8})$$

In principle, we can obtain Green function by the direct inversion of the matrix $E - \tilde{\mathcal{H}}$. However, the number of numerical operations required for the inversion of the matrix increases as N^3 with N the size of the matrix. We therefore need to reduce the size of matrix to inverse as small as possible.

Since we put the effective Hamiltonian $\tilde{\mathcal{H}}_{N_p+1}$ on the upper-left corner of the full Hamiltonian (Eq.(A1)), the sub-matrix G_{N_p+1, N_p+1} contains all information of the transport. This sub-matrix can be calculated as

$$G_{N_p+1, N_p+1} = \frac{1}{E - \tilde{\mathcal{H}}_{N_p+1} - \Gamma_{N_p+1}}, \quad (\text{A9})$$

where

$$\Gamma_{i+1} = V_{i+1, i} \frac{1}{E - \mathcal{H}_i - \Gamma_i} V_{i+1, i}^\dagger \quad (\text{for } i = 1, 2, \dots, N_p), \quad (\text{A10})$$

with

$$\Gamma_1 = V'_{1, C} \frac{1}{E - \mathcal{H}^C} V'^{\dagger}_{1, C}. \quad (\text{A11})$$

The inverse matrix of $E - \mathcal{H}^C$ can be calculated recursively[19] and each row of the matrix $V'_{1,C}$ contains only one non-zero element corresponding to the matrix element between neighbouring slices, which greatly simplifies the calculation of Γ_1 . In the calculation of Γ_{i+1} for $i = 1, 2, \dots, N_p$ and G_{N_p+1, N_p+1} , we need to inverse directly the matrix whose size is $(N_w^D + N_w^R + N_w^L) \times (N_w^D + N_w^R + N_w^L)$. This is much smaller than the original size of $E - \tilde{\mathcal{H}}$.

G_{N_p+1, N_p+1} consists of 9 parts.

$$G_{N_p+1, N_p+1} = \begin{pmatrix} G^{DD} & G^{DR} & G^{DL} \\ G^{RD} & G^{RR} & G^{RL} \\ G^{LD} & G^{LR} & G^{LL} \end{pmatrix} \quad (\text{A12})$$

where G^{IJ} ($I, J = D, R$ and L) is the Green function from the probe J to I . The scattering matrix can be calculated easily from the Green function [19].

-
- [1] S.A. Wolf *et al.*, Science **294**, 1488 (2001).
 - [2] I. Zutic, J. Fabian and S.D. Sarma, Rev. Mod. Phys. **76**, 323 (2004).
 - [3] G. Dresselhaus, Phys. Rev. **100**, 580 (1955).
 - [4] E.I. Rashba, Sov. Phys. Solid State **2**, 1109 (1960).
 - [5] Y.A. Bychkov and E.I. Rashba, J. Phys. C **17**, 6039 (1984).
 - [6] G. Lommer, F. Malcher and U. Rössler, Phys. Rev. Lett. **60**, 728 (1988).
 - [7] J. Nitta, T. Akazaki, H. Takayanagi and T. Enoki, Phys. Rev. Lett. **78**, 1335 (1997).
 - [8] G. Engels, J. Lange, Th. Schäpers and H. Lüth, Phys. Rev. B **55**, R1958 (1997).
 - [9] S. Datta and B. Das, Appl. Phys. Lett. **56**, 665 (1990).
 - [10] G. Schmidt, D. Ferrand, L.W. Molenkamp, A.T. Filip and B.J. van Wees, Phys. Rev. B **62**, R4790 (2000).
 - [11] L.D. Landau and E.M. Lifshitz, *Quantum mechanics: non-relativistic theory*, 3d ed., Pergamon Press, New York, (1991).
 - [12] A.A. Kiselev and K.W. Kim, Appl. Phys. Lett. **78**, 775 (2001).
 - [13] A.A. Kiselev and K.W. Kim, J. Appl. Phys. **94**, 4001 (2003).
 - [14] M. Governale and U. Zülicke, Phys. Rev. B **66**, 073311 (2002).
 - [15] C.W.J. Beenakker, Rev. Mod. Phys. **69**, 731 (1997).
 - [16] S. Pramanik, S. Bandyopadhyay and M. Cahay, cond-mat/0403021.

- [17] T. Ando, Phys. Rev. B **40**, 5325 (1989).
- [18] R. Landauer, IBM J. Res. Dev. **1**, 223 (1957).
- [19] T. Ando, Phys. Rev. B **44**, 8017 (1991).
- [20] T. Kawarabayashi and T. Ohtsuki, Phys. Rev. B **51**, 10897 (1995).
- [21] T. Kawarabayashi and T. Ohtsuki, Phys. Rev. B **67**, 165309 (2003).
- [22] M. Suzuki, Phys. Lett. A **146**, 319 (1990).
- [23] C.-M. Hu, C. Zehnder, Ch. Heyn and D. Heitmann, Phys. Rev. B **67**, 201302(R) (2003).